Physics Letters B 723 (2013) 1–6

Contents lists available at SciVerse ScienceDirect

Physics Letters B

www.elsevier.com/locate/physletb

Constraints on dark energy from the Lyα forest baryon acoustic oscillations measurement of the redshift 2.3 Hubble parameter

Omer Farooq *, Bharat Ratra

Department of Physics, Kansas State University, 116 Cardwell Hall, Manhattan, KS 66506, USA

ARTICLE INFO

Article history:
Received 14 February 2013
Received in revised form 25 March 2013
Accepted 22 April 2013
Available online 27 April 2013
Editor: S. Dodelson

ABSTRACT

We use the Busca et al. (2012) [11] measurement of the Hubble parameter at redshift $z = 2.3$ in conjunction with 21 lower z measurements, from Simon, Verde, and Jimenez (2005) [81], Gaztañaga, Cabré, and Hui (2009) [33], Stern et al. (2010) [85], and Moresco et al. (2012) [52], to place constraints on model parameters of constant and time-evolving dark energy cosmological models. The inclusion of the new Busca et al. (2012) [11] measurement results in $H(z)$ constraints significantly more restrictive than those derived by Farooq, Mania, and Ratra (2013) [31]. These $H(z)$ constraints are now more restrictive than those that follow from current Type Ia supernova (SNIa) apparent magnitude measurements Suzuki et al. (2012) [86]. The $H(z)$ constraints by themselves require an accelerating cosmological expansion at about 2 σ confidence level, depending on cosmological model and Hubble constant prior used in the analysis. A joint analysis of $H(z)$, baryon acoustic oscillation peak length scale, and SNIa data favors a spatially-flat cosmological model currently dominated by a time-independent cosmological constant but does not exclude slowly-evolving dark energy density.

1. Introduction

Observations indicate the cosmological expansion is accelerating now and that the Universe is spatially flat, provided the dark energy density responsible for the acceleration is close to or time independent. For reviews of dark energy see [9,40,45,93], and references therein.[1]

In the "standard" spatially-flat ΛCDM cosmological model [54] dark energy — Einstein's cosmological constant Λ — contributes a little more than 70% of the current energy budget. Nonrelativistic cold dark matter (CDM) is the next largest contributer (at a little more than 20%), followed by nonrelativistic baryonic matter (around 5%). See [68] and references therein for reviews of the standard model. It has been known for a while that the standard ΛCDM model is reasonably compatible with most observational constraints (see, e.g., [1,27,39,94]).[2] In the ΛCDM model the dark energy density is constant in time and does not vary in space.

It is well known that the standard ΛCDM model has some puzzling features that are easier to accept in a model in which the dark energy density is a slowly-decreasing function of time [55,67]. For recent discussions of time-varying dark energy models see [5,10,13,25,36,37,65,80,95], and references therein. In this Letter we study two dark energy models (with dark energy being either a cosmological constant or a slowly-evolving scalar field ϕ) as well as a dark energy parameterization.

In the ΛCDM model, time-independent dark energy density (the cosmological constant Λ) is modeled as a spatially homogeneous fluid with equation of state $p_\Lambda = -\rho_\Lambda$ that relates the fluid pressure and energy density. The XCDM parameterization has often been used to describe slowly-decreasing dark energy density. In this case dark energy is modeled as a spatially homogeneous X-fluid with equation of state $p_X = w_X \rho_X$. Here p_X and ρ_X are the pressure and energy density of the X-fluid and the equation of state parameter $w_X < -1/3$ is independent of time. When $w_X = -1$ the XCDM parameterization reduces to the complete, consistent ΛCDM model. For all other values of $w_X < -1/3$ the XCDM parameterization is incomplete as it does not describe spatial inhomogeneities (see, e.g. [63,66]). For computational simplicity, in the XCDM case we consider only a spatially-flat cosmological model.

The ϕCDM model is the simplest, complete and consistent model of slowly-decreasing dark energy density [55,67]. Here dark energy is modeled as the gradually decreasing (in ϕ and time) potential energy density $V(\phi)$ of the scalar field. In this Letter

* Corresponding author.
E-mail addresses: omer@phys.ksu.edu (O. Farooq), ratra@phys.ksu.edu (B. Ratra).

[1] Instead of dark energy that dominates the current cosmological energy budget, a less likely possibility is that these observations are an indication that general relativity needs to be modified on cosmological length scales. See [9,17,84], and references therein, for reviews of modified gravity. Here we assume that general relativity is an adequate description of cosmological gravitation.

[2] Note, however, that there are tentative observational indications that the "standard" CDM structure formation model, which is assumed in the ΛCDM model, might need modification (e.g., [56,58]).

0370-2693/$ – see front matter
http://dx.doi.org/10.1016/j.physletb.2013.04.044

we assume an inverse power-law potential energy density $V(\phi) \propto \phi^{-\alpha}$, where α is a nonnegative constant [55]. When $\alpha = 0$ the ϕCDM model reduces to the corresponding ΛCDM model. For computational simplicity, we assume a spatially-flat cosmology for ϕCDM.

Cosmological observations that provide the strongest evidence for dark energy are: SNIa apparent magnitude versus redshift data ([3,46,70,86] and references therein); cosmic microwave background (CMB) anisotropy measurements (e.g., [42,62]) combined with low estimates of the cosmological mass density ([20] and references therein), provided the dark energy density is close to or time independent; and, baryon acoustic oscillation (BAO) peak length scale data (e.g., [2,7,8,51]). Current error bars associated with these three types of data are still too large to allow for a significant observational discrimination between the ΛCDM model and the two simple time-varying dark energy models discussed above. Additional data are needed for this task, as well as to provide a cross check on the above results.

Other data that have been used for this purpose include look-back time as a function of redshift ([26,72,88,90] and references therein), gamma-ray burst luminosity distance as a function of redshift (e.g. [12,64,75,91]), strong gravitational lensing ([16,18,44,96] and references therein), HII starburst galaxy apparent magnitude as a function of redshift (e.g., [50,59,60]), angular size as a function of redshift ([23,38,47] and references therein), and galaxy cluster properties (e.g., [15,28,29,34]). The constraints from these data are, at present, significantly weaker than those from SNIa, BAO, and CMB anisotropy measurements, but it is anticipated that future data of these kinds will provide significant constraints.[3]

Two other current data sets provide interesting constraints on cosmological parameters, somewhat comparable to those from SNIa, BAO, and CMB anisotropy data. These are galaxy cluster gas mass fraction as a function of redshift measurements (e.g., [1,48, 74,82,89]) and measurements of the Hubble parameter as a function of redshift (e.g., [4,22,30,41,43,71,73,78,79,92]). Interestingly, most measurements now provide largely compatible constraints on cosmological parameters that are consistent with a currently accelerating cosmological expansion. This provides confidence that the broad outlines of a standard cosmological model are now in place.

In this Letter we use the 21 $H(z)$ measurements of [33,52,81, 85] (listed in Table 1 of [31]), in conjunction with the $H(z = 2.3)$ measurement of [11], determined from BAO in the Lyα forest (in combination with WMAP CMB anisotropy data, [42]), to constrain the ΛCDM and ϕCDM models and the XCDM parametrization. The inclusion of the new [11] measurement results in tighter constraints than those derived by [31] from the 21 $H(z)$ measurements alone. The new $H(z)$ constraints derived here are more restrictive than those derived from the recent SNIa data compilation of [86], which more carefully accounts for the systematic errors in SNIa measurements.[4] In addition to deriving $H(z)$ data only constraints, we also use these $H(z)$ measurements in combination with recent SNIa and BAO data to jointly constrain cosmological parameters. Adding the $H(z)$ data tightens the constraints, quite significantly in some parts of parameter space. More precisely, the $H(z)$ measurements more significantly tighten constraints on the nonrelativistic matter density parameter than on the parameter that more closely controls the time evolution of the dark energy density. Of course, the addition of CMB anisotropy data can greatly improve the constraints on the parameters of dark energy models, but this needs to be done in a joint analysis that is left for future work.

Our Letter is organized as follows. In Section 2 we present the basic equations of the three dark energy models we consider. Constraints from the data are derived in Section 3. We conclude in Section 4.

2. Dark energy models

In this section we list relevant characteristics of the two models (ΛCDM and ϕCDM) and the one parametrization (XCDM) we use in our analyses of the data.

In the ΛCDM model with spatial curvature the Hubble parameter evolves as

$$H(z; H_0, \mathbf{p}) = H_0\big[\Omega_{m0}(1+z)^3 + \Omega_\Lambda + (1-\Omega_{m0}-\Omega_\Lambda)(1+z)^2\big]^{1/2}, \quad (1)$$

where H_0 is the current value of Hubble parameter (the Hubble constant), the current value of the spatial curvature density parameter is $\Omega_{K0} = 1 - \Omega_{m0} - \Omega_\Lambda$, and the model parameter set we want to constrain is $\mathbf{p} = (\Omega_{m0}, \Omega_\Lambda)$. Here Ω_{m0} is the nonrelativistic (baryonic and cold dark) matter density parameter and Ω_Λ is the time-independent cosmological constant density parameter. Below we shall have need for the dimensionless Hubble parameter $E(z) = H(z)/H_0$.

The XCDM parameterization Friedmann equation is

$$H(z; H_0, \mathbf{p}) = H_0\big[\Omega_{m0}(1+z)^3 + (1-\Omega_{m0})(1+z)^{3(1+\omega_X)}\big]^{1/2}, \quad (2)$$

where for computational simplicity we consider only flat spatial hypersurfaces and the model parameters $\mathbf{p} = (\Omega_{m0}, \omega_X)$. The XCDM parametrization is incomplete, as it cannot describe the evolution of energy density inhomogeneities.

The ϕCDM model [55] is the simplest, complete and consistent dynamical dark energy model. In this model dark energy is a slowly-rolling scalar field ϕ with an, e.g., inverse-power-law potential energy density $V(\phi) = \kappa m_p^2 \phi^{-\alpha}$ where $m_p = 1/\sqrt{G}$ is the Planck mass, G is the Newtonian gravitational constant, and α is a nonnegative free parameter that determines κ. The scalar field part of the ϕCDM model action is

$$S = \frac{m_p^2}{16\pi}\int \sqrt{-g}\left(\frac{1}{2}\, g^{\mu\nu}\partial_\mu\phi\partial_\nu\phi - \kappa m_p^2\phi^{-\alpha}\right) d^4x, \quad (3)$$

where $g^{\mu\nu}$ is the metric tensor and α and κ are related as

$$\kappa = \frac{8}{3}\left(\frac{\alpha+4}{\alpha+2}\right)\left(\frac{2\alpha(\alpha+2)}{3}\right)^{\alpha/2}, \quad (4)$$

with corresponding scalar field equation of motion

$$\ddot{\phi} + 3\frac{\dot{a}}{a}\dot{\phi} - \kappa\alpha m_p^2\phi^{-(\alpha+1)} = 0, \quad (5)$$

where the overdot denotes a derivative with respect to time. In the spatially-flat case the Friedmann equation for the ϕCDM model is

$$H(z; H_0, \mathbf{p}) = H_0\big[\Omega_{m0}(1+z)^3 + \Omega_\phi(z,\alpha)\big]^{1/2}, \quad (6)$$

where $\Omega_\phi(z,\alpha)$ is determined by the ϕ field energy density

$$\rho_\phi = \frac{m_p^2}{16\pi}\left(\frac{1}{2}\dot{\phi}^2 + \kappa m_p^2\phi^{-\alpha}\right). \quad (7)$$

[3] In addition to soon to be available CMB anisotropy data from Planck, future space-based SNIa, BAO-like, and galaxy cluster measurements (e.g., [6,49,53,61,76, 77]) should soon provide interesting constraints on cosmological parameters.

[4] The study of $H(z)$ data is a much less-developed field than that of SNIa data, so it is not impossible that future $H(z)$ error bars might be larger than what we have used in our analysis here.

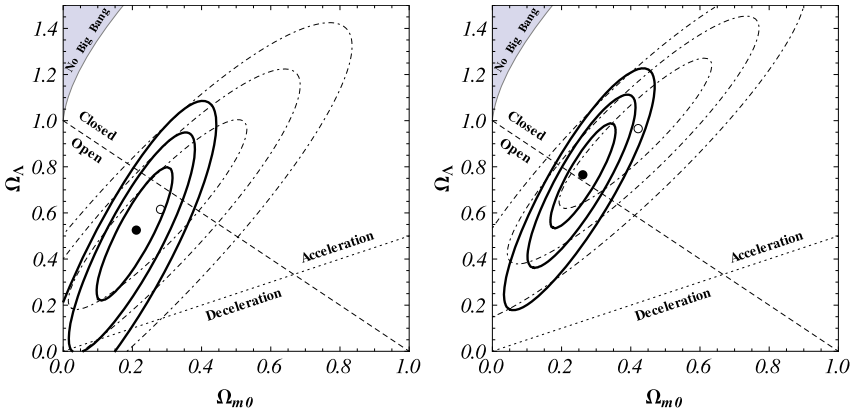

Fig. 1. Thick solid (thin dot-dashed) lines correspond to 1, 2, and 3 σ constraint contours from the new (old [31]) $H(z)$ data for the ΛCDM model. The filled (empty) circle is the best-fit point from the new (old) $H(z)$ data. The left panel is for the $H_0 = 68 \pm 2.8$ km s^{-1} Mpc^{-1} prior and the right panel is for the $H_0 = 73.8 \pm 2.4$ km s^{-1} Mpc^{-1} one. The dashed diagonal lines correspond to spatially-flat models, the dotted lines demarcate zero-acceleration models, and the shaded area in the upper left-hand corners are the region for which there is no big bang. The filled circles correspond to best-fit pair $(\Omega_{m0}, \Omega_\Lambda) = (0.21, 0.53)$ with $\chi^2_{\rm min} = 15.1$ (left panel) and best-fit pair $(\Omega_{m0}, \Omega_\Lambda) = (0.26, 0.77)$ with $\chi^2_{\rm min} = 16.1$ (right panel). The empty circles correspond to best-fit pair $(\Omega_{m0}, \Omega_\Lambda) = (0.28, 0.62)$ with $\chi^2_{\rm min} = 14.6$ (left panel) and best-fit pair $(\Omega_{m0}, \Omega_\Lambda) = (0.42, 0.97)$ with $\chi^2_{\rm min} = 14.6$ (right panel).

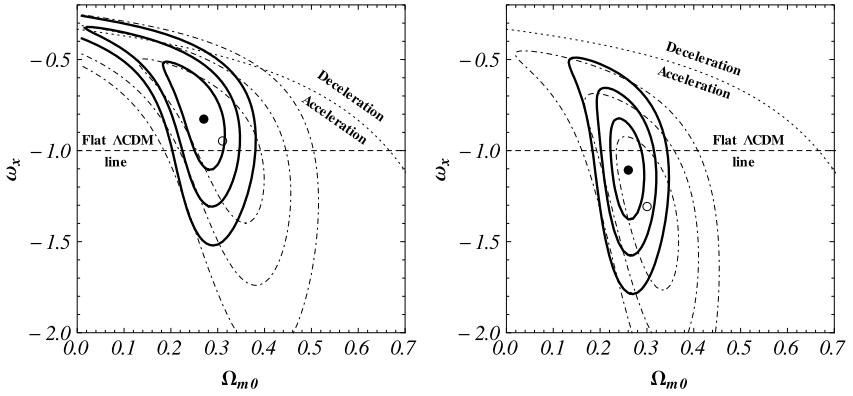

Fig. 2. Thick solid (thin dot-dashed) lines correspond to 1, 2, and 3 σ constraint contours from the new (old [31]) $H(z)$ data for the XCDM model. The filled (empty) circle is the best-fit point from the new (old) $H(z)$ data. The left panel is for the $H_0 = 68 \pm 2.8$ km s^{-1} Mpc^{-1} prior and the right panel is for the $H_0 = 73.8 \pm 2.4$ km s^{-1} Mpc^{-1} one. The dashed horizontal lines at $\omega_{\rm X} = -1$ correspond to spatially-flat ΛCDM models and the curved dotted lines demarcate zero-acceleration models. The filled circles correspond to best-fit pair $(\Omega_{m0}, \omega_{\rm X}) = (0.27, -0.82)$ with $\chi^2_{\rm min} = 15.2$ (left panel) and best-fit pair $(\Omega_{m0}, \omega_{\rm X}) = (0.36, -1.1)$ with $\chi^2_{\rm min} = 15.9$ (right panel). The empty circles correspond to best-fit pair $(\Omega_{m0}, \omega_{\rm X}) = (0.31, -0.94)$ with $\chi^2_{\rm min} = 14.6$ (left panel) and best-fit pair $(\Omega_{m0}, \omega_{\rm X}) = (0.30, -1.30)$ with $\chi^2_{\rm min} = 14.6$ (right panel).

Eqs. (5)–(7) constitute a system of differential equations which can be solved numerically for the ϕCDM model Hubble parameter $H(z)$, using the initial conditions described in [55]. In this case the model parameter set is $\mathbf{p} = (\Omega_{m0}, \alpha)$.

3. Constraints from the data

We first study $H(z)$ data constraints on cosmological parameters. To the 21 independent $H(z)$ data points listed in Table 1 of [31] we add the [11] $H(z = 2.3) = 224 \pm 8$ km s^{-1} Mpc^{-1} measurement, determined from BAO in the Lyα forest (in conjunction with WMAP CMB anisotropy data [42]).

To constrain cosmological parameters $\mathbf{p}$ of the models of interest we follow the procedure of [31]. We again marginalize over the nuisance parameter H_0 using two different Gaussian priors with $\bar{H}_0 \pm \sigma_{H_0} = 68 \pm 2.8$ km s^{-1} Mpc^{-1} and with $\bar{H}_0 \pm \sigma_{H_0} = 73.8 \pm 2.4$ km s^{-1} Mpc^{-1}. As discussed there, the Hubble constant measurement uncertainty can significantly affect cosmological parameter estimation (for a recent example see, e.g., [14]). The lower of the two values we use is from a median statistics analysis [35] of 553 measurements of H_0 [21]; this estimate has been stable for over a decade now [19,35]. The other value is a recent, HST based one [69]. Other recent estimates are compatible with at least one of the two values we use (see, e.g., [24,32,83,87]).

We maximize the likelihood $\mathcal{L}_H(\mathbf{p})$ with respect to the parameters $\mathbf{p}$ to find the best-fit parameter values $\mathbf{p_0}$. In the models we consider $\chi^2_H = -2\ln[\mathcal{L}_H(\mathbf{p})]$ depends on two parameters. We define 1, 2, and 3 σ confidence intervals as two-dimensional parameter sets bounded by $\chi^2_H(\mathbf{p}) = \chi^2_H(\mathbf{p_0}) + 2.3$, $\chi^2_H(\mathbf{p}) = \chi^2_H(\mathbf{p_0}) + 6.17$, and $\chi^2_H(\mathbf{p}) = \chi^2_H(\mathbf{p_0}) + 11.8$, respectively.

Figs. 1–3 show the constraints from the $H(z)$ data derived here, as well as those derived by [31], for the three dark energy models, and for the two different H_0 priors. Clearly, the H $(z = 2.3)$ measurement of [11] significantly tightens the constrains. Given that the nonrelativistic matter density is larger relative to the dark energy density at $z = 2.3$, it is perhaps not unexpected that the [11] measurement tightens the constraints on Ω_{m0} much more significantly than it does for the constraints on the other parameter which more strongly affects the evolution of the dark energy density, see Figs. 2 and 3.

Comparing the $H(z)$ constraints derived here, and shown in Figs. 1–3 here, to the SNIa constraints shown in Fig. 4 of [31], we see that the new $H(z)$ data constraints are significantly more restrictive than those that follow on using the SNIa data. This is a remarkable result. Qualitatively, because of the dependence on the

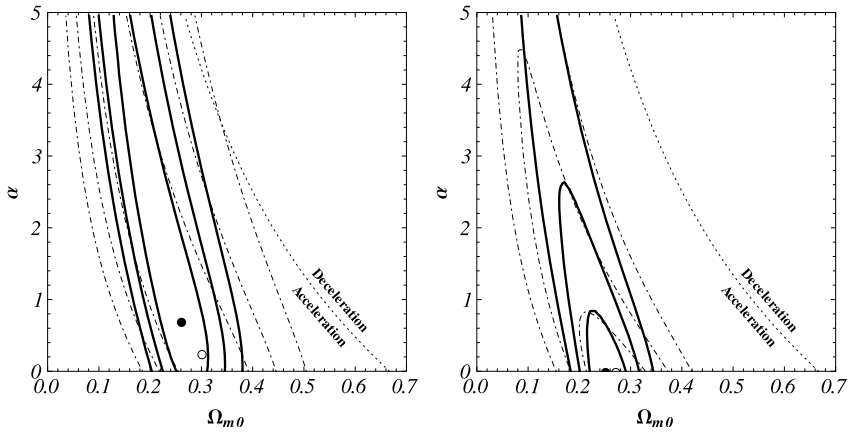

Fig. 3. Thick solid (thin dot-dashed) lines correspond to 1, 2, and 3 σ constraint contours from the new (old [31]) $H(z)$ data for the ϕCDM model. The filled (empty) circle is the best-fit point from the new (old) $H(z)$ data. The left panel is for the $H_0 = 68 \pm 2.8$ km s^{-1} Mpc^{-1} prior and the right panel is for the $H_0 = 73.8 \pm 2.4$ km s^{-1} Mpc^{-1} one. The horizontal axes at $\alpha = 0$ correspond to spatially-flat ΛCDM models and the curved dotted lines demarcate zero-acceleration models. The filled circles correspond to best-fit pair $(\Omega_{m0}, \alpha) = (0.36, 0.70)$ with $\chi^2_{\rm min} = 15.2$ (left panel) and best-fit pair $(\Omega_{m0}, \alpha) = (0.25, 0)$ with $\chi^2_{\rm min} = 16.1$ (right panel). The empty circles correspond to best-fit pair $(\Omega_{m0}, \alpha) = (0.30, 0.25)$ with $\chi^2_{\rm min} = 14.6$ (left panel) and best-fit pair $(\Omega_{m0}, \alpha) = (0.27, 0)$ with $\chi^2_{\rm min} = 15.6$ (right panel).

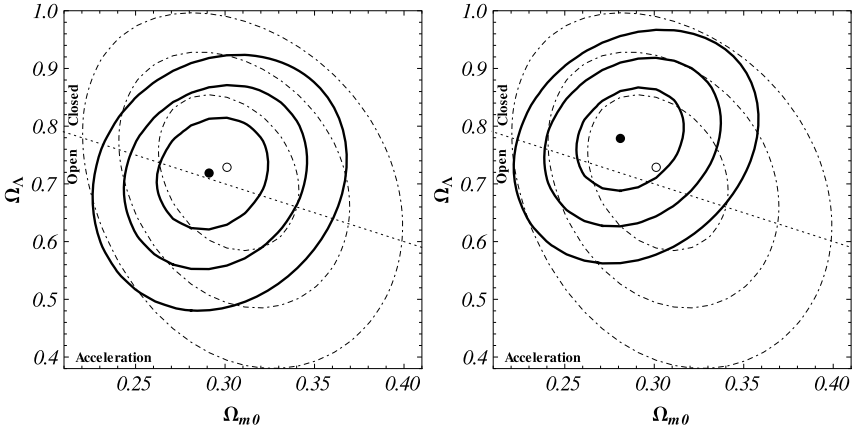

Fig. 4. Thick solid (thin dot-dashed) lines are 1, 2, and 3 σ constraint contours for the ΛCDM model from a joint analysis of the BAO and SNIa (with systematic errors) data, with (without) the $H(z)$ data. The full (empty) circle marks the best-fit point determined from the joint analysis with (without) the $H(z)$ data. The dotted sloping line corresponds to spatially-flat ΛCDM models. In the left panel we use the $H_0 = 68 \pm 2.8$ km s^{-1} Mpc^{-1} prior. Here the empty circle [no $H(z)$ data] corresponds to best-fit pair $(\Omega_{m0}, \Omega_\Lambda) = (0.30, 0.73)$ with $\chi^2_{\rm min} = 551$ while the full circle [with $H(z)$ data] indicates best-fit pair $(\Omega_{m0}, \Omega_\Lambda) = (0.29, 0.72)$ with $\chi^2_{\rm min} = 567$. In the right panel we use the $H_0 = 73.8 \pm 2.4$ km s^{-1} Mpc^{-1} prior. Here the empty circle [no $H(z)$ data] corresponds to best-fit pair $(\Omega_{m0}, \Omega_\Lambda) = (0.30, 0.73)$ with $\chi^2_{\rm min} = 551$ while the full circle [with $H(z)$ data] demarcates best-fit pair $(\Omega_{m0}, \Omega_\Lambda) = (0.28, 0.78)$ with $\chi^2_{\rm min} = 568$.

H_0 prior and on the model used in the analysis, Figs. 1–3 show that the $H(z)$ data alone require accelerated cosmological expansion at approximately the two standard deviation confidence level.

While the $H(z)$ data provide tight constraints on a linear combination of cosmological parameters, the banana-like constraint contours of Figs. 1–3 imply that these data alone cannot significantly discriminate between cosmological models. To tighten the constraints we must add other data to the mix. Following [31], we derive constraints on cosmological parameters of the three models from a joint analysis of the $H(z)$ data with the 6 BAO peak length scale measurements of [7,57], and [8], and the Union2.1 compilation of 580 SNIa apparent magnitude measurements (covering a redshift range $0.015 < z < 1.4$) from [86].

Figs. 4–6 show the constraints on cosmological parameters for the ΛCDM and ϕCDM models and the XCDM parametrization, from a joint analysis of the BAO and SNIa data, as well as from a joint analysis of the BAO, SNIa, and $H(z)$ data. Including the $H(z)$ data in the analysis tightens the constraints, somewhat significantly (sometimes by more than two standard deviations), in parts of the parameter spaces. Fig. 7 shows the $H(z)$ data and the two best-fit ΛCDM models. The $H(z)$ data do support the idea of a deceleration to acceleration transition somewhere in the range $0.5 < z < 1$.

Table 1 lists the two standard deviation bounds on the individual cosmological parameters, determined from their one-dimensional posterior probability distributions functions (which are derived by marginalizing the two-dimensional likelihood over the other cosmological parameter).

4. Conclusion

Adding the [11] $z = 2.3$ measurement of the Hubble parameter, from BAO in the Lyα forest, to the 21 $H(z)$ data points tabulated in [31], results in an $H(z)$ data set that provides quite restrictive constraints on cosmological parameters. These constraints are tighter than those that follow from the SNIa data of [86], which carefully accounts for all known systematic uncertainties. The $H(z)$ field is much less mature than the SNIa one, and there might be some as yet undetected $H(z)$ systematic errors that could broaden the $H(z)$ error bars, as has happened in the SNIa case. However, we emphasize that the observers have done a careful analysis and the error bars we have used in our analysis have been carefully estimated.

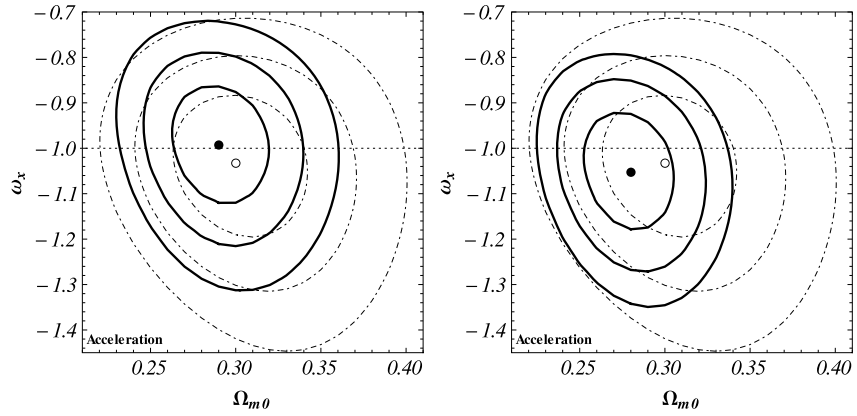

Fig. 5. Thick solid (thin dot-dashed) lines are 1, 2, and 3 σ constraint contours for the XCDM parametrization from a joint analysis of the BAO and SNIa (with systematic errors) data, with (without) the $H(z)$ data. The full (empty) circle marks the best-fit point determined from the joint analysis with (without) the $H(z)$ data. The dotted horizontal line at $\omega_X = -1$ corresponds to spatially-flat ΛCDM models. In the left panel we use the $H_0 = 68 \pm 2.8$ km s^{-1} Mpc^{-1} prior. Here the empty circle [no $H(z)$ data] corresponds to best-fit pair $(\Omega_{m0}, \omega_X) = (0.30, -1.03)$ with $\chi^2_{\rm min} = 551$, while the full circle [with $H(z)$ data] demarcates best-fit pair $(\Omega_{m0}, \omega_X) = (0.29, -0.99)$ with $\chi^2_{\rm min} = 568$. In the right panel we use the $H_0 = 73.8 \pm 2.4$ km s^{-1} Mpc^{-1} prior. Here the empty circle [no $H(z)$ data] corresponds to best-fit pair $(\Omega_{m0}, \omega_X) = (0.30, -1.03)$ with $\chi^2_{\rm min} = 551$ while the full circle [with $H(z)$ data] indicates best-fit pair $(\Omega_{m0}, \omega_X) = (0.28, -1.05)$ with $\chi^2_{\rm min} = 569$.

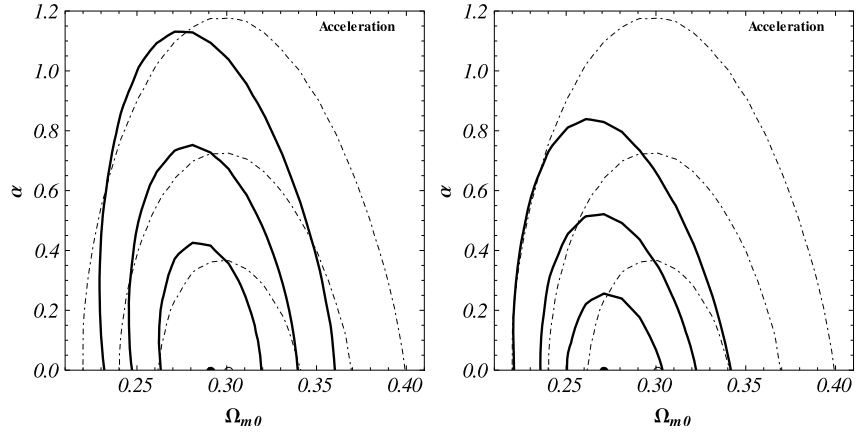

Fig. 6. Thick solid (thin dot-dashed) lines are 1, 2, and 3 σ constraint contours for the ϕCDM model from a joint analysis of the BAO and SNIa (with systematic errors) data, with (without) the $H(z)$ data. The full (empty) circle marks the best-fit point determined from the joint analysis with (without) the $H(z)$ data. The $\alpha = 0$ horizontal axes correspond to spatially-flat ΛCDM models. In the left panel we use the $H_0 = 68 \pm 2.8$ km s^{-1} Mpc^{-1} prior. Here the empty circle corresponds to best-fit pair $(\Omega_{m0}, \alpha) = (0.30, 0)$ with $\chi^2_{\rm min} = 551$ while the full circle indicates best-fit pair $(\Omega_{m0}, \alpha) = (0.29, 0)$ with $\chi^2_{\rm min} = 567$. In the right panel we use the $H_0 = 73.8 \pm 2.4$ km s^{-1} Mpc^{-1} prior. Here the empty circle corresponds to best-fit pair $(\Omega_{m0}, \alpha) = (0.30, 0)$ with $\chi^2_{\rm min} = 551$ while the full circle demarcates best-fit pair $(\Omega_{m0}, \alpha) = (0.27, 0)$ with $\chi^2_{\rm min} = 569$.

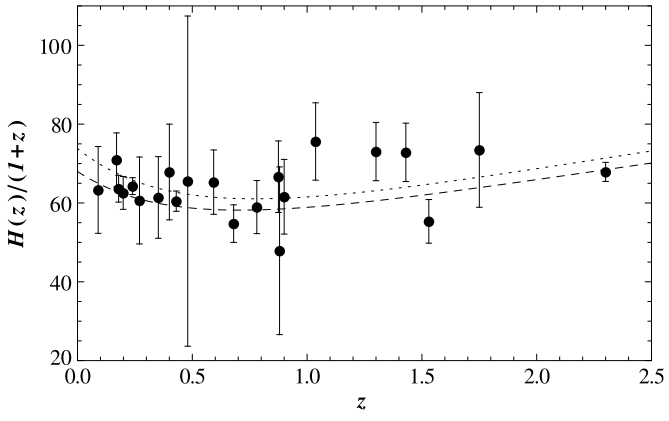

Fig. 7. Measurements and predictions for $H(z)/(1+z)$ as a function of z. Dashed (dotted) lines show the predictions for the best-fit ΛCDM model from the combined BAO, SNIa, and $H(z)$ data analyses, with cosmological parameter values $(\Omega_{m0}, \Omega_\Lambda, h) = (0.29, 0.72, 0.68)[(0.28, 0.78, 0.738)]$.

In addition to providing more restrictive constraints, the $H(z)$ data alone requires accelerated cosmological expansion at the current epoch at approximately 2 σ confidence level, depending on model and H_0 prior used in the analysis.

In summary, the results of the joint analysis of the $H(z)$, BAO, and SNIa data are quite consistent with the predictions of the stan-

Table 1
Two standard deviation bounds on cosmological parameters using BAO + SNIa and BAO + SNIa + $H(z)$ data, for three models and two H_0 priors.

Model and prior	BAO + SNIa	BAO + SNIa + $H(z)$
ΛCDM, $h = 0.68 \pm 0.028$	$0.25 < \Omega_{m0} < 0.36$ $0.53 < \Omega_\Lambda < 0.89$	$0.26 < \Omega_{m0} < 0.33$ $0.60 < \Omega_\Lambda < 0.84$
ΛCDM, $h = 0.738 \pm 0.024$	$0.25 < \Omega_{m0} < 0.36$ $0.53 < \Omega_\Lambda < 0.89$	$0.25 < \Omega_{m0} < 0.32$ $0.66 < \Omega_\Lambda < 0.89$
XCDM, $h = 0.68 \pm 0.028$	$0.30 < \Omega_{m0} < 0.38$ $-1.18 < \omega_X < -0.78$	$0.27 < \Omega_{m0} < 0.32$ $-1.03 < \omega_X < -0.77$
XCDM, $h = 0.738 \pm 0.024$	$0.30 < \Omega_{m0} < 0.38$ $-1.18 < \omega_X < -0.78$	$0.25 < \Omega_{m0} < 0.30$ $-1.15 < \omega_X < -0.90$
ϕCDM, $h = 0.68 \pm 0.028$	$0.25 < \Omega_{m0} < 0.35$ $0 < \alpha < 0.54$	$0.25 < \Omega_{m0} < 0.32$ $0 < \alpha < 0.56$
ϕCDM, $h = 0.738 \pm 0.024$	$0.25 < \Omega_{m0} < 0.35$ $0 < \alpha < 0.54$	$0.25 < \Omega_{m0} < 0.30$ $0 < \alpha < 0.21$

dard spatially-flat ΛCDM cosmological model, with current energy budget dominated by a time-independent cosmological constant. However, currently-available data cannot rule out slowly-evolving dark energy density. We anticipate that soon to be available better quality data will more clearly discriminate between constant and slowly-evolving dark energy density.

Acknowledgements

We thank Data Mania and Larry Weaver for useful discussions and helpful advice. This work was supported in part by DOE grant DEFG03-99EP41093 and NSF grant AST-1109275.

References

[1] S.W. Allen, et al., MNRAS 383 (2008) 879.
[2] L. Anderson, et al., arXiv:1203.6594 [astro-ph.CO], 2012.
[3] P. Astier, R. Pain, C. R. Physique 13 (2012) 521.
[4] A. Aviles, et al., Phys. Rev. D 86 (2012) 123516.
[5] S. Basilakos, D. Polarski, J. Solà, Phys. Rev. D 86 (2012) 043010.
[6] T. Basse, et al., arXiv:1205.0548 [astro-ph.CO], 2012.
[7] F. Beutler, et al., MNRAS 416 (2011) 3077.
[8] C. Blake, et al., MNRAS 418 (2011) 1707.
[9] Yu.L. Bolotin, O.A. Lemets, D.A. Yerokhin, arXiv:1108.0203 [astro-ph.CO], 2011.
[10] P. Brax, A.-C. Davis, Phys. Lett. B 707 (2012) 1.
[11] N.G. Busca, et al., arXiv:1211.2616 [astro-ph], 2012.
[12] V.C. Busti, R.C. Santos, J.A.S. Lima, Phys. Rev. D 85 (2012) 103503.
[13] R.-G. Cai, et al., Phys. Rev. D 86 (2012) 023511.
[14] E. Calabrese, et al., Phys. Rev. D 86 (2012) 043520.
[15] L. Campanelli, et al., Eur. Phys. J. C 72 (2012) 2218.
[16] S. Cao, et al., J. Cosmology Astropart. Phys. 1203 (2012) 016.
[17] S. Capozziello, M. De Laurentis, Phys. Rept. 509 (2011) 167.
[18] K.-H. Chae, et al., Astrophys. J. 607 (2004) L71.
[19] G. Chen, J.R. Gott, B. Ratra, PASP 115 (2003) 1269.
[20] G. Chen, B. Ratra, PASP 115 (2003) 1143.
[21] G. Chen, B. Ratra, PASP 123 (2011) 1127.
[22] G. Chen, B. Ratra, Phys. Lett. B 703 (2011) 406.
[23] Y. Chen, B. Ratra, Astron. Astrophys. 543 (2012) A104.
[24] M. Colless, F. Beutler, C. Blake, arXiv:1211.2570 [astro-ph.CO], 2012.
[25] F.E.M. Costa, J.A.S. Lima, F.A. Oliveira, arXiv:1204.1864 [astro-ph.CO], 2012.
[26] M.A. Dantas, et al., Phys. Lett. B 699 (2011) 239.
[27] T.M. Davis, et al., Astrophys. J. 666 (2007) 716.
[28] C. De Boni, et al., arXiv:1205.3163 [astro-ph.CO], 2012.
[29] N.C. Devi, T.R. Choudhury, A.A. Sen, arXiv:1112.0728 [astro-ph.CO], 2011.
[30] X. Duan, Y. Li, C. Gao, arXiv:1111.3423 [astro-ph.CO], 2011.
[31] O. Farooq, D. Mania, B. Ratra, Astrophys. J. 764 (2013) 138.
[32] W.L. Freedman, et al., Astrophys. J. 758 (2012) 24.
[33] E. Gaztañaga, A. Cabré, L. Hui, MNRAS 399 (2009) 1663.
[34] A.H. Gonzalez, et al., Astrophys. J. 753 (2012) 163.
[35] J.R. Gott, et al., Astrophys. J. 549 (2001) 1.
[36] J.A. Gu, C.-C. Lee, C.-Q. Geng, Phys. Lett. B 718 (2013) 722.
[37] L. Hollenstein, et al., Phys. Rev. D 85 (2012) 124031.
[38] J.C. Jackson, arXiv:1207.0697 [astro-ph.CO], 2012.
[39] H.K. Jassal, J.S. Bagla, T. Padmanabhan, MNRAS 405 (2010) 2639.
[40] R. Jimenez, Fortschr. Phys. 59 (2011) 602.
[41] R. Jimenez, et al., Astrophys. J. 593 (2003) 622.
[42] E. Komatsu, et al., Astrophys. J. Suppl. Ser. 192 (2011) 18.
[43] S. Kumar, MNRAS 422 (2012) 2532.
[44] S. Lee, K.-W. Ng, Phys. Rev. D 76 (2007) 043518.
[45] M. Li, et al., Commun. Theor. Phys. 56 (2011) 525.
[46] X.-D. Li, et al., J. Cosmology Astropart. Phys. 1107 (2011) 011.
[47] J.A.S. Lima, J.V. Cunha, arXiv:1206.0332 [astro-ph.CO], 2012.
[48] J. Lu, et al., Eur. Phys. J. C 71 (2011) 1800.
[49] E. Majerotto, et al., MNRAS 424 (2012) 1392.
[50] D. Mania, B. Ratra, Phys. Lett. B 715 (2012) 9.
[51] K.T. Mehta, et al., arXiv:1202.0092 [astro-ph.CO], 2012.
[52] M. Moresco, et al., J. Cosmology Astropart. Phys. 1208 (2012) 006.
[53] A. Pavlov, L. Samushia, B. Ratra, Astrophys. J. 760 (2012) 19.
[54] P.J.E. Peebles, Astrophys. J. 284 (1984) 439.
[55] P.J.E. Peebles, B. Ratra, Astrophys. J. 325 (1988) L17.
[56] P.J.E. Peebles, B. Ratra, Rev. Mod. Phys. 75 (2003) 559.
[57] W.J. Percival, et al., MNRAS 401 (2010) 2148.
[58] L. Perivolaropoulos, J. Phys. Conf. Ser. 222 (2010) 012024.
[59] M. Plionis, et al., AIP Conf. Proc. 1241 (2010) 267.
[60] M. Plionis, et al., MNRAS 416 (2011) 2981.
[61] S. Podariu, P. Nugent, B. Ratra, Astrophys. J. 553 (2001) 39.
[62] S. Podariu, et al., Astrophys. J. 559 (2001) 9.
[63] S. Podariu, B. Ratra, Astrophys. J. 532 (2000) 109.
[64] V. Poitras, J. Cosmology Astropart. Phys. 1206 (2012) 039.
[65] J. Ponce de Leon, Class. Quant. Grav. 29 (2012) 135009.
[66] B. Ratra, Phys. Rev. D 43 (1991) 3802.
[67] B. Ratra, P.J.E. Peebles, Phys. Rev. D 37 (1988) 3406.
[68] B. Ratra, M.S. Vogeley, PASP 120 (2008) 235.
[69] A.G. Riess, et al., Astrophys. J. 730 (2011) 119.
[70] E.J. Ruiz, et al., Phys. Rev. D 86 (2012) 103004.
[71] L. Samushia, G. Chen, B. Ratra, arXiv:0706.1963 [astro-ph], 2007.
[72] L. Samushia, et al., Phys. Lett. B 693 (2010) 509.
[73] L. Samushia, B. Ratra, Astrophys. J. 650 (2006) L5.
[74] L. Samushia, B. Ratra, Astrophys. J. 680 (2008) L1.
[75] L. Samushia, B. Ratra, Astrophys. J. 714 (2010) 1347.
[76] L. Samushia, et al., MNRAS 410 (2011) 1993.
[77] B. Sartoris, et al., MNRAS 423 (2012) 2503.
[78] M. Seikel, et al., Phys. Rev. D 86 (2012) 083001.
[79] A.A. Sen, R.J. Scherrer, Phys. Lett. B 659 (2008) 457.
[80] A. Sheykhi, et al., Intl. J. Theo. Phys. 51 (2012) 1663.
[81] J. Simon, L. Verde, J. Jimenez, Phys. Rev. D 71 (2005) 123001.
[82] F.C. Solano, U. Nucamendi, arXiv:1207.0250 [astro-ph.CO], 2012.
[83] J.G. Sorce, R.B. Tully, H.M. Courtois, Astrophys. J. 758 (2012) L12.
[84] G.D. Starkman, Phil. Trans. Roy. Soc. Lond. A 369 (2011) 5018.
[85] D. Stern, et al., J. Cosmology Astropart. Phys. 1002 (2010) 008.
[86] N. Suzuki, et al., Astrophys. J. 746 (2012) 85.
[87] G.A. Tammann, B. Reindl, arXiv:1211.4655 [astro-ph.CO], 2012.
[88] S. Thakur, et al., arXiv:1204.2617 [astro-ph.CO], 2012.
[89] M. Tong, H. Noh, Eur. Phys. J. C 71 (2011) 1586.
[90] D. Tonoiu, A. Caramete, L.A. Popa, Rom. Rep. Phys. 63 (2011) 879.
[91] F.Y. Wang, J.G. Dai, Astron. Astrophys. 536 (2011) A96.
[92] H. Wang, T.J. Zhang, Astrophys. J. 748 (2012) 111.
[93] Y. Wang, AIP Conf. Proc. 1458 (2012) 285.
[94] K.M. Wilson, G. Chen, B. Ratra, Mod. Phys. Lett. A 21 (2006) 2197.
[95] L. Xu, Y. Wang, H. Noh, Eur. Phys. J. C 72 (2012) 1931.
[96] Q.-J. Zhang, Y.-L. Wu, J. Cosmology Astropart. Phys. 1008 (2010) 038.